

Optical Properties of Short Range Ordered Arrays of Nanometer Gold Disks Prepared by Colloidal Lithography

Per Hanarp,* Mikael Käll, and Duncan S. Sutherland

Department of Applied Physics, Chalmers University of Technology, S-41296 Göteborg, Sweden

Received: November 26, 2002; In Final Form: April 11, 2003

The optical properties of gold nanodisk arrays prepared by colloidal lithography are studied experimentally. The arrays exhibit short range translational order and weak interparticle interactions. Tunable localized surface plasmon resonances are achieved by varying the diameter of the disks at constant disk height. The macroscopic optical properties are well-described by modeling the gold disks as oblate spheroids in the electrostatic limit. The optical sensing capabilities of the disks are investigated by varying the surrounding refractive index. It is found, in agreement with theory, that more oblate disk shapes have higher sensitivity. This suggests that nanodisks prepared by colloidal lithography are of interest as substrates for optimizing optical biosensing methods at the nanometer scale.

Introduction

The optical properties of noble metal nanostructures have given possibilities for many new nanooptical devices,¹ in particular substrates for highly sensitive optical detection of biomolecule adsorption through surface-enhanced Raman spectroscopy and nanoparticle surface plasmon resonance spectroscopy.^{2–9} The main cause of the brilliant optical properties of noble metal nanoparticles is the excitation of collective electron oscillations that are strongly coupled to the optical field. These resonances, which are often called localized surface plasmon resonances, sensitively depend on particle shape, size, composition, and the optical properties of the surrounding medium. When a nanoparticle is excited at its resonance wavelength, strong absorption and/or scattering of the incident light and a concurrent local electric field enhancement occurs.¹⁰ Because of their ability to focus light at nanometer length scales, metal nanoparticles can be utilized for applications that require subwavelength resolution and/or amplification of electromagnetic processes.

There is currently considerable interest in the fabrication and optical characterization of gold and silver particles on solid supports. Such structures have important potential as substrates for surface plasmon enhanced spectroscopies,³ but studies focusing on a detailed understanding of how the nanostructure parameters influence the localized surface plasmon resonance are of both fundamental and applied interest. Recent studies include investigations of the optical properties of nanoparticles of different shapes,^{11–14} holes in optically thick metal films,¹⁵ elongated rods,^{16,17} and core–shell particles.¹⁸ Ordered arrays of nanoparticles can be prepared by, for example, nanosphere lithography^{13,19} and electron beam lithography.^{12,14} In these studies, it was found that the interparticle spacing is critical to both the plasmon resonance wavelength and its damping properties. This is due to a combination of near-field coupling between evanescent fields from particles situated within a few tens of nanometers from each other and far-field interference between dipolar fields from distant particles.¹⁴ In the design of any particle plasmon application or experiment, one thus has

to consider both the influence of the particle array and the properties of the individual particles. In most practical applications, one will utilize an ensemble of particles, which means that one also has to take into account the polydispersity in particle size and shape and associated inhomogeneous broadening effects.

In this work, we focus on the optical properties of short range ordered arrays of nanometer gold disks. Our aim is to investigate, and if possible separate, the influence of the array structure (i.e., interparticle spacing) and the individual particle geometry on the resultant plasmon excitations. We have therefore chosen the colloidal lithography nanofabrication method.^{20–22} This is a novel method to fabricate optically active nanostructures,²³ capable of producing large areas (>cm²) of individual gold disks with controlled size, shape, and interparticle spacing. The arrays have well-defined short range ordering but no long range order, which should minimize the effect of array dipolar plasmon coupling.¹⁴ A simple electrostatic spheroid model is used to interpret the results and to discuss the physical background of the observed effects. In particular, we show that the disks in the short range ordered arrays essentially act as individual light scatterers and that the plasmon resonance wavelength and its sensitivity to the surrounding medium can be tuned by disk shape.

Materials and Methods

Gold disks were prepared on soda glass surfaces using colloidal lithography^{20–22} as illustrated in Figure 1. The procedure was as follows: (i) Polystyrene colloidal particles (0.1–0.5%, 20–110 nm sulfate-modified latex, Interfacial Dynamics Corporation, U.S.A.) were deposited by electrostatic self-assembly onto glass slides precoated with 20 nm of Au (for details on the particle adsorption, see ref 20). The resulting particle saturation coverages have well-defined structure with short range ordering due to electrostatic interparticle repulsion. The interparticle separation was controlled by the salt concentration in the colloidal solution (NaCl, 0–0.5 mM). (ii) The shape and size of the adsorbed polystyrene particles were modified by heat treatment (hotplate 106–120 °C for 2 min) and in some cases an oxygen plasma treatment (PlasmaTherm Batchtop VII

* To whom correspondence should be addressed. E-mail: hanarp@fy.chalmers.se.

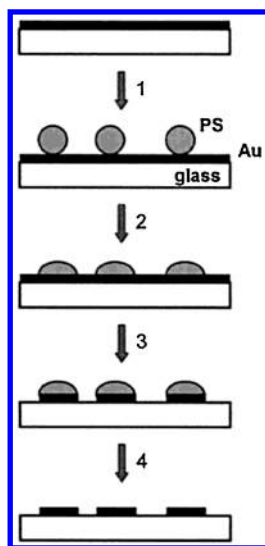


Figure 1. Nanofabrication of gold dots using colloidal lithography. (1) Polystyrene nanoparticles are adsorbed by polyelectrolyte self-assembly onto a glass slide precoated with 20 nm of Au. (2) Shape modification of the polystyrene particles by heat treatment on a hotplate, 106–120 °C. (3) Ar ion beam etching. (4) Removal of particle by UV/ozone, leaving gold disks on a glass substrate.

RIE/PE, 50 W, 250 mTorr, 0–33 s). (iii) Ar ion beam etching (Oxford model 300 Ion Beam Etching System, 500 V, 200 mA, 90 s) was used to remove the Au film, utilizing the particle film as an etch mask. (iv) The remains of the polystyrene particles were removed by a UV/ozone treatment and a subsequent water rinse, leaving separated oblate gold disks on the glass.

Standard UV/vis/NIR optical extinction measurements were performed on a Cary 500 spectrophotometer, using a sampling area of approximately 0.7 cm². Optical data were then averaged over $\sim 10^9$ – 10^{10} individual disks. Measurements in different refractive index liquids were done by subsequently exchanging soluble liquids in varying order. The following refractive index environments were used: N₂ gas ($n = 1.00$), water (1.33), acetone (1.36), 2-propanol (1.38), 1,1,1-trichloroethane (1.44), and *p*-xylene (1.50). In each series, a final measurement in N₂ environment showed that the plasmon resonance peak position returned to the initial value. In the following, we define the optical extinction spectrum as $E(\lambda) = 1 - I(\lambda)/I_0(\lambda)$, where $I_0(\lambda)$ is the incident light and $I(\lambda)$ is the transmitted light. The extinction spectra are analyzed for peak position, height, and half-width. These experimentally determined parameters are directly transferable to the localized surface plasmon resonance wavelength, cross-section, and damping, respectively. After the optical measurements, the morphology of each individual sample was characterized using atomic force microscopy (AFM) and scanning electron microscopy (SEM) to determine the height, diameter, average spacing, and number density of the gold disks. The details of the characterization of the particle films were reported previously.^{20,24} Briefly, SEM images were analyzed with image analysis software (Scion Image, MD) to determine the particle radius, area, and *x,y* coordinates. The interparticle spacing was determined by calculating radial distribution functions from these data (see Figure 2b). The radial distribution function is defined as $g(r) = \rho(r)/\rho_0$, where $\rho(r)$ is the average concentration of particle centers in a thin circular shell with radius r around a particle and ρ_0 is the average concentration of particles on the whole surface. X-ray photoelectron spectroscopy (XPS) was used to characterize the chemical homogeneity of the samples and to ascertain that the Au between the

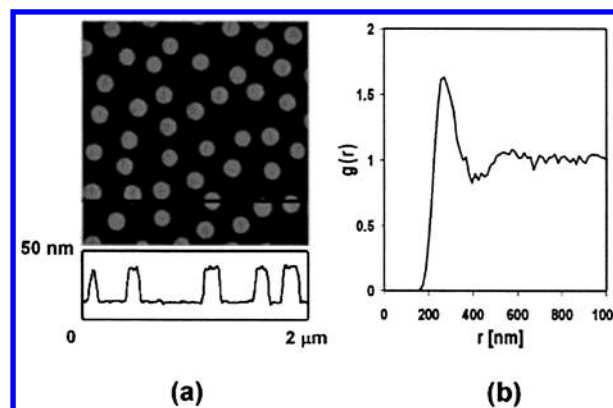


Figure 2. Characterization of the gold disk arrays. (a) AFM image and topographical line scan of gold disks on a glass substrate. Sample details: height, 20 nm; diameter, 140 nm; and interparticle spacing, 280 nm. Note that the disk diameter appears to be larger due to AFM tip-broadening effects. (b) Radial distribution function of the same sample. The primary peak at 280 nm (center-to-center distance) shows the short range ordering of the disks. The constant value at longer distances indicates the lack of long range order.

TABLE 1: List of Approximate Sample Geometries Used in This Work

diameter (nm)	height (nm)	spacing (nm)
20	20	80
70	20	130
70	20	180
70–150	20	280

disks was completely removed during the etching process. Overetching for 30 s gave only trace amounts of Au left.

Results and Discussion

Figure 2a shows a typical AFM image of the nanoparticles together with a topographical linescan. It is evident that the resulting structure is disk-shaped. SEM images from the side have shown that the walls of the disks are slightly inclined, i.e., the disk base is slightly larger than the diameter of the upper surface. This is a result of the etching process and of a concurrent etching and slow shrinkage of the masking polystyrene particles. The standard deviation in the gold disk diameter and height is ± 6 – 10 and ± 1 nm, respectively, which is comparable to samples prepared by, for example, electron beam lithography.^{12,14} The array of disks is short range ordered (see Figure 2) with a characteristic distance between neighboring disks controlled by the polystyrene particle adsorption conditions in the fabrication procedure.²⁰ The characteristic short range interparticle spacing is seen as a peak in the radial distribution function (see Figure 2b).

Table 1 lists the approximate geometrical details of the samples used in this work. The interparticle spacing ranged from 80 to 280 nm (center-to-center) for disk diameters of 20–150 nm. The average edge-to-edge distance is approximately equal to the particle diameter or larger for all samples. Repeated fabrication of identical samples showed good reproducibility in particle size and shape, in array nanogeometry, and in the corresponding optical properties.

In Figure 3, we show extinction spectra and SEM images for three different particle spacings, approximately 130 ± 20 , 180 ± 30 , and 280 ± 50 nm, respectively (the indicated variations are the stochastic spread in the interparticle spacings), while keeping the disk diameter ≈ 70 nm and height 20 nm constant. As can be seen, there is an excellent agreement in peak position and a very similar peak shape for the three

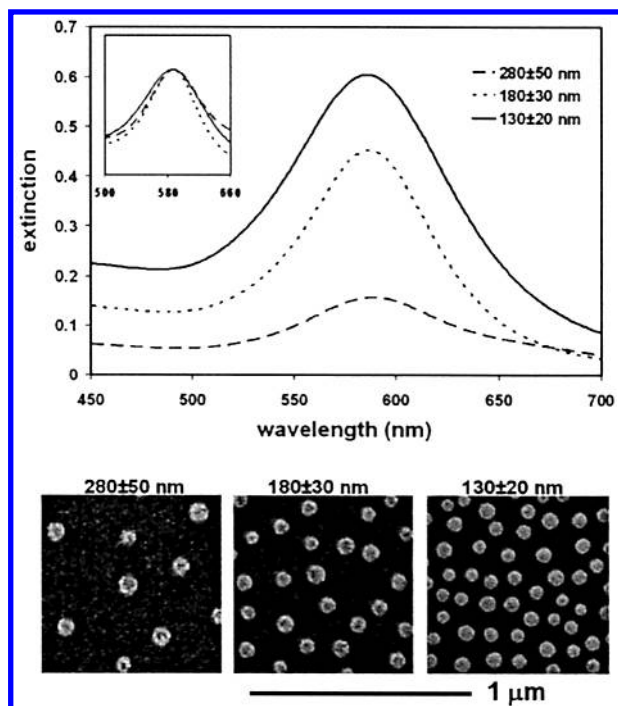


Figure 3. Optical extinction spectra and SEM images for ≈ 70 nm diameter, 20 nm high Au dots with three average spacings between neighboring particles, approximately 130 ± 20 , 180 ± 30 , and 280 ± 50 nm, respectively. Inset: the peaks normalized to the same height.

samples. This shows that the interparticle interactions only have a weak effect within the investigated range of interparticle spacings. We attribute the lack of far-field coupling to the random long range arrangement of particles in samples made by colloidal lithography and that the spacings studied are well below the resonance wavelengths for the disks. On the other hand, the spacings studied are all sufficiently large to avoid strong near-field coupling between the evanescent fields. We are thus essentially observing single particle properties in the experiment. It should be noted that in a standard diffraction setup with the colloidal lithography samples we find no evidence for coherent far-field diffraction or “grating effects”. Instead, we find forward transmission of colored light with no clear angular dependence.

A number of sophisticated electrodynamics models and techniques have been used in order to interpret the optical properties of metal nanoparticles.²⁵ In the following, we choose the simplest available model that gives qualitative agreement with data, namely, to approximate the disks as individual dipoles in the electrostatic limit. The induced dipole moment $p = \epsilon_m \alpha E$, where E is the applied plane-wave electric field and ϵ_m is the dielectric constant of the surrounding material, is then determined by the dipole polarizability α . Approximating the disks as oblate spheroids, with radii $a = b > c$ and with the light incident perpendicular to the major axis yields, yields²⁶

$$\alpha = 4\pi a^2 c \frac{\epsilon_1 - \epsilon_m}{3\epsilon_m + 3L_a(\epsilon_1 - \epsilon_m)} \quad (1)$$

Here, ϵ_1 is the dielectric function of the spheroid, and L_a is a geometrical factor that is a function of the a/c aspect ratio. The condition for plasmon resonance is then

$$\text{Re}(3\epsilon_m + 3L_a(\epsilon_1 - \epsilon_m)) = 0 \quad (2)$$

To compare with the experimental data, we calculate the

extinction and elastic scattering cross-sections:

$$\sigma_{\text{ext}} = k \text{Im}(\alpha), \quad \sigma_{\text{sca}} = \frac{k^4}{6\pi} |\alpha|^2 \quad (3)$$

where $k = 2\pi(\epsilon_m)^{1/2}/\lambda$ is the wave-vector of the incident light. The experimental dielectric function of gold according to Johnson and Christy²⁷ is used for ϵ_1 . We have accounted for the gold disks that are situated on a glass substrate (refractive index, $n_{\text{glass}} = 1.52$) surrounded on all other sides by air ($n_{\text{air}} = 1.00$), by using an effective refractive index of $n_{\text{eff}} = 1.26$.¹¹

The electrostatic spheroid theory gives good agreement with data when it comes to the absolute position of the localized surface plasmon peak, as discussed below, but severely underestimates the peak width for the larger particles. This difference can be accounted for by including a correction for radiation damping due to spontaneous emission from the induced dipole.^{25,28} The radiation damping correction can be introduced through a renormalized dipole polarizability

$$\alpha^* = \frac{\alpha}{\left(1 - \frac{2}{12\pi} ik^3 \alpha\right)} \quad (4)$$

which is then inserted in to eq 3 to obtain a modified expression for the extinction cross-section

$$\sigma_{\text{ext,rd}} = \frac{\sigma_{\text{ext}} + \sigma_{\text{sca}}}{1 + \frac{k^2}{3\pi} \left(\sigma_{\text{ext}} + \frac{1}{2} \sigma_{\text{sca}}\right)} \quad (5)$$

Using eqs 1 and 3, we investigated the influence of polydispersity in the disks diameter, $d = 2a$, on the localized surface plasmon resonance. The inhomogeneous broadening effects estimated using the measured polydispersities indicate only a small influence on the plasmon resonance peak position, height, and half-width. For example, for a single spheroid with $a, b = 50$ nm and $c = 10$ nm, the peak position, height, and half-width are 625 nm, $0.99 \times 10^{-9} \text{ cm}^2$, and 0.11 eV, respectively, while for a square distribution of spheroids with $a, b = 45\text{--}55$ nm and $c = 10$ nm these parameters become 628 nm, $0.85 \times 10^{-9} \text{ cm}^2$, and 0.14 eV.

We now turn to the influence of disk shape on the plasmon resonance, as illustrated in Figure 4, where the extinction spectra and corresponding SEM images are shown for disks with varying diameters of 74, 92, 113, and 137 nm but with constant height 20 nm and constant number density $1.4 \times 10^9/\text{cm}^2$. The data show that there is a rapid redshift in the plasmon resonance wavelength and an increased extinction peak area/height with increasing disk diameter. Figure 5a summarizes the variation in peak position as a function of disk diameter. As can be seen, there is a linear dependence over the whole size range, with a slope of $\Delta\lambda_{\text{max}}/\Delta d = 1.6$. As a comparison, we modeled the extinction spectra using oblate spheroid theory with (solid line) and without (dashed line) the radiation damping correction. The resulting calculated peak positions are similar and in excellent agreement with the experimental results. The linear dependence can be understood by approximating the dielectric function of gold by $\epsilon_1 \approx k\lambda + m$, where k and m are real valued constants,²⁹ which is a reasonable assumption in the studied wavelength range. Using this expression for ϵ_1 in the condition for the plasmon resonance, eq 2 gives the plasmon resonance wavelength, $\lambda_{\text{spr}} = k^{-1}[(\epsilon_m/L_a) + \epsilon_m - m]$. This means that λ_{spr} is linearly dependent on L_a^{-1} . Furthermore, because L_a^{-1} is proportional to the aspect ratio a/c , we have that λ_{spr} has a linear

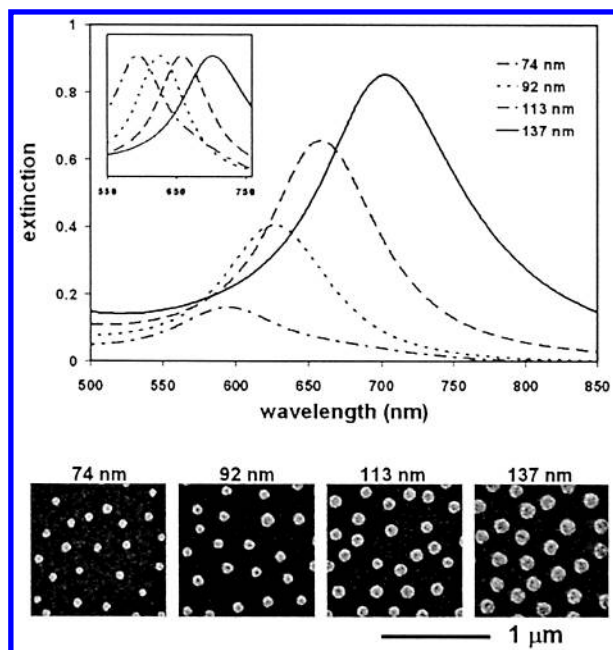


Figure 4. Optical extinction spectra and the corresponding SEM images for disks with varying diameters (74, 92, 113, and 137 nm) but with constant height (20 nm) and constant interparticle spacing (280 ± 50 nm). Inset: the peaks normalized to the same height.

dependence on the particle diameter since particle height is kept constant. Varying the particle diameter for a fixed height is thus a simple and predictable way to achieve a desired plasmon resonance wavelength.

Figure 5b shows the extinction cross-section per particle as a function of disk diameter. Experimental cross-sections were calculated from the measured extinction spectra using the relation

$$E = 1 - \frac{I}{I_0} = \sigma_{\text{ext}} N \quad (6)$$

where N is the particle number density on the surface. Here, we take peak height at resonance as a measure of E (using a linear background subtraction). The number density of particles is readily calculated from SEM images of the samples. As can be seen, there is a linear dependence in a logarithmic scale, indicating that the extinction is proportional to d^3 . The experimentally measured cross-sections are in reasonable agreement with calculations, with the best agreement for larger disks obtained by including the radiation damping correction. In addition, our measurements are in a similar range as a cross-section measured for the nanosphere lithography silver dots.³⁰ It should be noted that eq 6 is strictly valid for the two-dimensional arrays studied in this work provided that the extinction is $\ll 1$. If the extinction is close to 1 and the summed particle cross-sections therefore approach the total surface area, the individual particle cross-section will be significantly underestimated while the half-width will be overestimated. For diameters larger than 100 nm in Figure 5b,c, the extinction is larger than 0.5 and this is likely to have some influence on the measured cross-sections and half-widths.

Figure 5c illustrates the damping properties of the plasmon excitations, by plotting the dependence of peak half-width as a function of resonance energy. A plasmon can decay radiatively or nonradiatively, e.g., into electron-hole pairs. The half-width Γ of the excitation in the spectral domain gives a decay time τ in the time domain, $\tau = \hbar/\Gamma$. In Figure 5c, it can be seen that

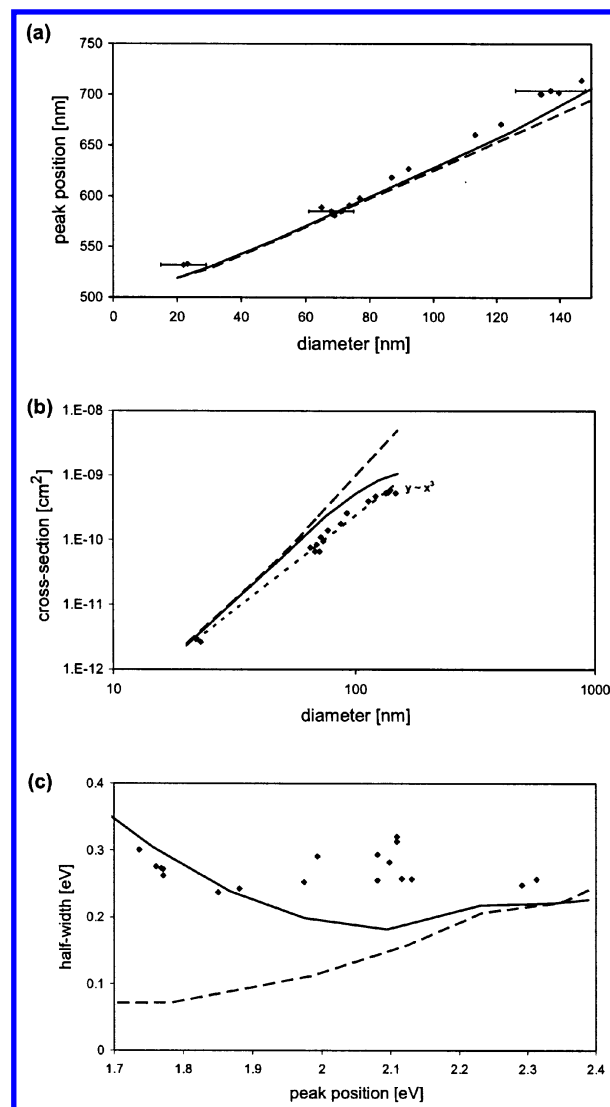


Figure 5. (a) Optical extinction peak position in air as a function of disk diameter. The dashed line indicates calculations using spheroid theory with an effective surrounding refractive index of 1.26, and the solid line is spheroid theory including radiation damping. Error bars indicate the spread of values in particle diameter. The error in determining the extinction peak position is smaller than the symbol size. (b) Optical extinction cross-section per particle (calculated as peak height/particle number density) as a function of diameter (note the logarithmic scale). The short dashed line is just a guide to the eye for the experimental data. (c) Optical extinction peak half-width as a function of peak position.

the experimental peak half-width is approximately constant and independent of plasmon energy (or aspect ratio). As a comparison, the purely electrostatic spheroid theory (dashed line) and a recent experimental study by Sönnichsen et al.³¹ show a strong decrease in half-width with decreasing plasmon energy. This insensitivity of peak width as a function of excitation energy in our experiments is, however, essentially reproduced in the theory corrected for radiation damping (solid line) and is thus likely an effect of the relatively large sizes of the disks studied and the increasing radiative damping for larger particles.

The optical field associated with the surface plasmon is strongest near the surface of the nanoparticles. This makes the resonance extremely sensitive to small changes in refractive index near the particle surface, a property that can be used for various nanosensing applications.^{2,7,8} We measured the change in plasmon peak position for gold dots of different aspect ratios

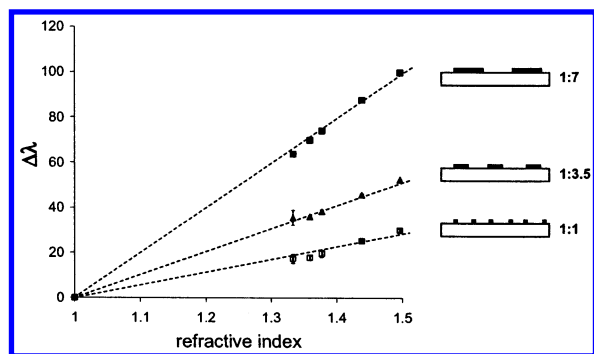


Figure 6. Optical extinction peak shift as a function of refractive index for disk aspect ratios 1, 3.5, and 7. The data demonstrate that the sensing capabilities of nanodisks can be tuned by varying the disk nanomorphology. The error bars indicate the spread of values for 2–3 independent measurements.

immersed in a range of different refractive index liquids (see Figure 6). We found that the extinction peak wavelength shifts linearly with surrounding refractive index as expected. In addition, in agreement with previous papers,^{32,33} the sensitivity to the local refractive index is strongly affected by the nanoparticle shape. Here, we find a substantially increased shift in peak position for more elongated disks; $d\lambda/dn = 60, 100$, and 200 nm/RIU for aspect ratios 1, 3.5, and 7, respectively. This can be compared to a sensitivity of 70 nm/RIU measured for 20 nm spherical gold particles immobilized on a glass substrate.⁹ The increased sensitivity for more oblate shapes is expected from the spheroid theory, where $d\lambda/dn \approx 2k^{-1}[(1/L_a) - 1]n$,²⁹ an expression derived from eq 2 using the approximate dielectric function, $\epsilon_1 \approx k\lambda + m$. The shape factor, L_a , decreases with increasing aspect ratio, thus resulting in a higher sensitivity for more oblate particle shapes.

Summary and Conclusions

In this work, we have presented a new, fast, and relatively simple method to prepare short range ordered arrays of gold disks with tunable localized surface plasmon resonances. We have investigated the variation in macroscopic optical properties of the disk arrays as a function of nanoparticle shape and found good agreement with single particle electrostatic spheroid theory including radiation damping. No evidence for dipolar plasmon interactions was observed for the arrays with short range order but lacking long range order. With increasing aspect ratio of the disks, we found a linear increase in plasmon resonance wavelength and an approximately constant peak-width. Moreover, we show that the sensitivity of the plasmon resonance wavelength to a change in surrounding refractive index is substantially increased for more elongated disks. The results suggest that these materials are of great interest as nanofabricated substrates for optimizing optical biosensing methods, such

as surface-enhanced Raman scattering or sensing methods based on the localized surface plasmon resonance change with refractive index.

References and Notes

- Andersen, P. C.; Rowlen, K. L. *Appl. Spectrosc.* **2002**, *56*, 124A–135A.
- Himmelhaus, M.; Takei, H. *Sens. Actuators B* **2000**, *63*, 24–30.
- Moskovits, M. *Rev. Mod. Phys.* **1985**, *57*, 783–826.
- Nie, S.; Emory, S. R. *Science* **1997**, *275*, 1102–1106.
- Xu, H.; Bjerneld, E. J.; Käll, M.; Börjesson, L. *Phys. Rev. Lett.* **1999**, *83*, 4357–4360.
- Wei, A.; Kim, B.; Sadtler, B.; Tripp, S. L. *ChemPhysChem* **2001**, *2*, 743–745.
- Nath, N.; Chilkoti, A. *Anal. Chem.* **2002**, *74*, 504–509.
- Haes, A. J.; Van Duyne, R. P. *J. Am. Chem. Soc.* **2002**, *124*, 10596–10604.
- Okamoto, T.; Yamaguchi, I.; Kobayashi, T. *Opt. Lett.* **2000**, *25*, 372–374.
- Kreibig, U.; Vollmer, M. *Optical Properties of Metal Clusters*; Springer-Verlag: Berlin, 1995.
- Gotschy, W.; Vonmetz, K.; Leitner, A.; Ausnegg, F. R. *Appl. Phys. B* **1996**, *63*, 381–384.
- Niklasson, G. A.; Bobbert, P. A.; Craighead, H. G. *Nanostruct. Mater.* **1999**, *12*, 725–730.
- Jensen, T. R.; Schatz, G. C.; Van Duyne, R. P. *J. Phys. Chem. B* **1999**, *103*, 2394–2401.
- Lamprecht, B.; Schider, G.; Lechner, R. T.; Ditlbacher, H.; Krenn, J. R.; Leitner, A.; Ausnegg, F. R. *Phys. Rev. Lett.* **2000**, *84*, 4721–4724.
- Ebbesen, T. W.; Lezec, H. J.; Ghaemi, H. F.; Thio, T.; Wolff, P. A. *Nature* **1998**, *391*, 667–669.
- Krenn, J. R.; Schider, G.; Rechberger, W.; Lamprecht, B.; Leitner, A.; Ausnegg, F. R. *Appl. Phys. Lett.* **2000**, *77*, 3379–3381.
- Link, S.; El-Sayed, M. A. *J. Phys. Chem. B* **1999**, *103*, 8410–8426.
- Oldenburg, S. J.; Jackson, J. B.; Westcott, S. L.; Halas, N. J. *Appl. Phys. Lett.* **1999**, *75*, 2897–2899.
- Haynes, C. L.; Van Duyne, R. P. *J. Phys. Chem. B* **2001**, *105*, 5599–5611.
- Hanarp, P.; Sutherland, D.; Gold, J.; Kasemo, B. *Colloids Surf. A* **2003**, *214*, 23–36.
- Hanarp, P.; Sutherland, D. S.; Gold, J.; Kasemo, B. *Nanostruct. Mater.* **1999**, *12*, 429–432.
- Sutherland, D. S.; Broberg, M.; Nygren, H.; Kasemo, B. *Macromol. Biosci.* **2001**, *1*, 270–273.
- Aizpurua, J.; Hanarp, P.; Sutherland, D. S.; Käll, M.; Bryant, G. W.; García de Abajo, F. J. *Phys. Rev. Lett.* **2003**, *90*, 057401.
- Hanarp, P.; Sutherland, D. S.; Gold, J.; Kasemo, B. *J. Colloid Interface Sci.* **2001**, *241*, 26–31.
- Kelly, K. L.; Coronado, E.; Zhao, L. L.; Schatz, G. C. *J. Phys. Chem. B* **2003**, *107*, 668–677.
- Bohren, C. F.; Huffman, D. R. *Absorption and Scattering of Light by Small Particles*; John Wiley & Sons: New York, 1983.
- Johnson, P. B.; Christy, R. W. *Phys. Rev. B* **1972**, *6*, 4370–4379.
- Wokaun, A.; Gordon, J. P.; Liao, P. F. *Phys. Rev. Lett.* **1982**, *48*, 957–960.
- Xu, H.; Käll, M. *Sens. Actuators B* **2002**, *87*, 244.
- Jensen, T. R.; Duval Malinsky, M.; Haynes, C. L.; Van Duyne, R. P. *J. Phys. Chem. B* **2000**, *104*, 10594–10556.
- Sönnichsen, C.; Franzl, T.; Wilk, T.; von Plessen, G.; Feldmann, J.; Wilson, O.; Mulvaney, P. *Phys. Rev. Lett.* **2002**, *88*, 077402.
- Sun, Y.; Xia, Y. *Anal. Chem.* **2002**, *74*, 5297–5305.
- Jensen, T. R.; Duval, M. L.; Kelly, K. L.; Lazarides, A. A.; Schatz, G. C.; Van Duyne, R. P. *J. Phys. Chem. B* **1999**, *103*, 9846–9853.